Finite Elements in Analysis and Design 143 (2018) 1–10

Contents lists available at ScienceDirect

Finite Elements in Analysis and Design

journal homepage: www.elsevier.com/locate/finel

Exploring the design space of nonlinear shallow arches with generalised path-following

B.S. Cox [a,*], R.M.J. Groh [a], D. Avitabile [b], A. Pirrera [a]

[a] Bristol Composites Institute (ACCIS), Department of Aerospace Engineering, University of Bristol, Queen's Building, University Walk, Bristol, BS8 1TR, UK
[b] School of Mathematical Sciences, University of Nottingham, University Park, Nottingham, NG7 2RD, UK

ARTICLE INFO

Keywords:
Arches
Bifurcation
Generalised path-following
Numerical continuation
Parametric analysis
Snap-through

ABSTRACT

The classic snap-through problem of shallow arches is revisited using the so-called *generalised path-following technique*. Classical buckling theory is a popular tool for designing structures prone to instabilities, albeit with limited applicability as it assumes a linear pre-buckling state. While incremental-iterative nonlinear finite element methods are more accurate, they are considered to be complex and costly for parametric studies. In this regard, a powerful approach for exploring the entire design space of nonlinear structures is the generalised path-following technique. Within this framework, a nonlinear finite element model is coupled with a numerical continuation solver to provide an accurate and robust way of evaluating multi-parametric structural problems. The capabilities of this technique are exemplified here by studying the effects of four different parameters on the structural behaviour of shallow arches, namely, mid span transverse loading, arch rise height, distribution of cross-sectional area along the span, and total volume of the arch. In particular, the distribution of area has a pronounced effect on the nonlinear load-displacement response and can therefore be used effectively for elastic tailoring. Most importantly, we illustrate the risks entailed in optimising the shape of arches using linear assumptions, which arise because the design drivers influencing linear and nonlinear designs are in fact topologically opposed.

1. Introduction

Structural nonlinearities, particularly those of an elastic nature, are gaining considerable momentum within engineering applications, and are being viewed as a positive design feature [1]. Nonlinear structural problems have been discussed in the literature for decades, however they are seldom exploited outside of the academic environment. This general reluctance engineers harbour for nonlinear structures is justified by two prevailing statements: (i) the lack of sufficiently robust computational tools, and (ii) the time-consuming nature of solving incremental-iterative problems, especially when multi-parametric studies for optimisation or imperfection sensitivity are conducted.

Across all length scales, slender and thin-walled structures are commonly used in engineering applications for a number of reasons. In micro- and meso-scale applications thin-walled structures are exploited for their ease of manufacture and ability to deform significantly without failure, thus providing unparalleled functionality that relies on nonlinear behaviour. In macro-scale applications, such as the aerospace and automotive sectors, thin-walled shell structures are used for their structural efficiency.

Although more efficient in their load carrying capacities, macro-scale thin-walled and slender structures are susceptible to structural instabilities. Small-scale structures relying on nonlinearities for functionality and large scale structures being prone to instabilities, it is evident that geometric nonlinearities need to be accounted for at all stages of the design process.

Arched structures, which are the focus of this paper, are known to exhibit instabilities and are a textbook example of classic snap-through buckling behaviour. In fact, snap-through instabilities of arched structures occur in a wide range of applications, from the tailorable design of micro-electromechanical systems (MEMS), to the meso-scale light-switch type structures, and further, to the failure of macro-scale civil structures.

Large scale arched structures, particularly those whose loading capacity is intrinsically linked to the deformations sustained, are particularly prone to instabilities. Carpinteri *et al.* [2] present an industrial

* Corresponding author.
E-mail addresses: Bradley.Cox@bristol.ac.uk (B.S. Cox), Rainer.Groh@bristol.ac.uk (R.M.J. Groh), Daniele.Avitabile@nottingham.ac.uk (D. Avitabile), Alberto.Pirrera@bristol.ac.uk (A. Pirrera).

https://doi.org/10.1016/j.finel.2018.01.004
Received 25 July 2017; Received in revised form 14 January 2018; Accepted 15 January 2018
Available online XXX

example illustrating the importance of nonlinear analysis for a modern roof-structure. Carpinteri concludes that current linear methods are insufficient in predicting the post-buckled state and, most importantly, the load-carrying capacity of the roof.

The same buckling behaviour is also observed on the micro-scale within the field of MEMS [3–5], a discipline which has seen significant growth in recent years. Micro-electromechanical systems provide a particularly challenging problem since the topic couples a number of disciplines, from solid and fluid mechanics to thermomechanics and electromagnetism. All of these fields can introduce their own forms of nonlinearity and these can interact in a complex manner to yield emergent phenomena that are difficult to predict.

Established methods for exploring a nonlinear design space require onerous parametric studies. With the application of the generalised path-following technique, however, the design space can be evaluated within a single solution process, for any number of parameters.

1.1. History of arched beam structures

Concave load-bearing structures are one of the oldest structures known to man. In this sense, a clear demarcation between *masonry arches* introduced in antiquity, *i.e.* concave structures constructed by a series of rigid building blocks joined with little to no tensile loading, and *elastic arches*, capable of resisting both membrane forces and bending moments, is necessary. For a fascinating history of arch construction, and its theoretical development from arch theory to computational mechanics, the interested reader is directed to chapter 4 of reference [6]. Throughout this paper we refer to compliant elastic arches which use snap-through for functionality and hence the research presented herein is restricted to slender arches. Such compliant arches, which utilise elastic snap-through "failure" well before plastic deformations occur, are being used in MEMS devices [7] and for novel metamaterials [8].

The critical buckling of shallow arches, either by symmetric snap-through or by an asymmetric bifurcation, is a seemingly well-understood problem. Once the solution space is opened up to more parameters beyond a simple load factor, however, it quickly becomes apparent that this problem is more intricate and complex than at first sight.

1.2. Generalised path-following in structural mechanics

There appears to be little question that the so-called incremental-iterative methods represent by far the most popular procedures for the solution of nonlinear continuum mechanics. Conventional path-following techniques are based on a single parameter, either: displacement [9,10], load [11,12], external work [13,14], arc-length [15–18], or others [19], and these result in a single load-displacement curve, as illustrated in Fig. 1a. This curve is, however, only a single equilibrium locus on a multi-dimensional solution manifold parametrised by any number of other variables that can influence the behaviour of the structure, *e.g.* material properties, geometric dimensions, imperfections, *etc.* Hence, traditional arc-length methods available in commercial finite element solvers are degenerate cases of a *generalised path-following technique* restricted to the forcing parameter-displacement space, and it is cumbersome or impossible to change two or more parameters simultaneously, which for example is required for tracking bifurcations. Whereby the only parameter that can be actively varied in these commercial solvers is the loading factor. The capabilities of a generalised path-following technique exceed those of conventional path-following methods by enabling visualisation of the structure's behaviour in multi-dimensional space. This technique allows *any* number of parameters to be continued, *i.e.* treated akin to a loading factor, during a single solution run and thus eliminates the necessity for extensive parametric studies.

Historically, the generalised path-following technique has been used extensively in the fields of applied mathematics and physics [20–23], where the term *numerical continuation* is a more common designation. In structural engineering applications, however, *path-following* is a familiar term and therefore *generalised path-following*, as introduced by Eriksson and co-workers [24], is a more intuitive designation as it differentiates from conventional path-following in load-displacement space.

In the 1960's Sewell introduced the notion of the equilibrium surface [25], whose shape could be used to identify the stability of the underlying structure with respect to changes in the governing parameters. With the advent of catastrophe theory in structural mechanics this interest intensified, mostly in an analytical setting [26–28], but a generalised computational framework was not introduced to the community until the 1980's by Rheinboldt [29–31]. The concepts introduced by

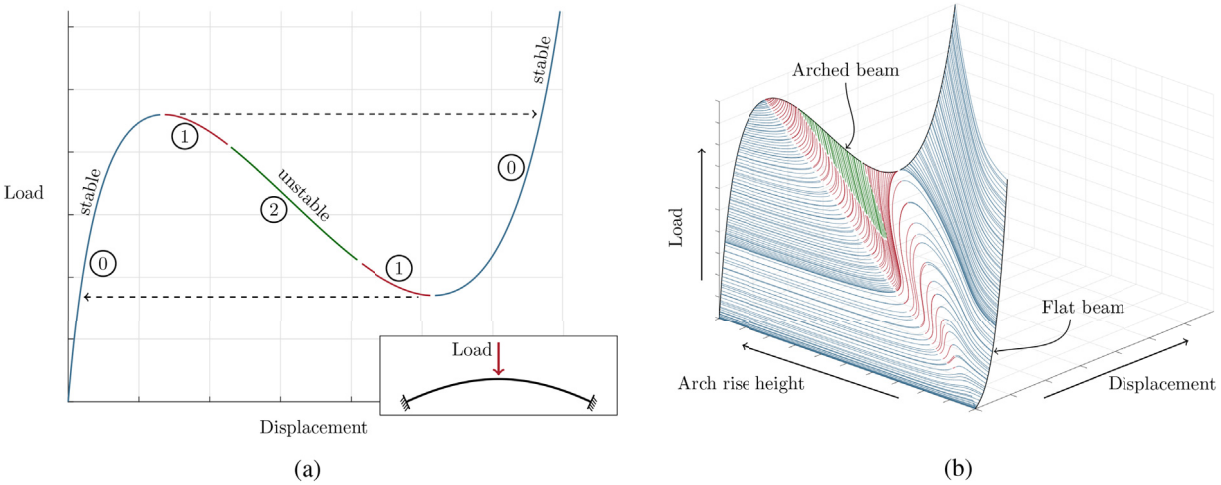

Fig. 1. (a) Fundamental equilibrium path for a baseline case of an arched beam, illustrating classic snap-through behaviour. Numbers and colours on curve segments denote the degree of instability; (b) A solution surface created by the generalised path following technique, here the arch rise height is varied from zero to a predefined maximum. The colours on curve segments, once again, denote the degree of instability. On both figures the different colour segments are separated by critical points, where the stability of the structure with respect to the loading parameter changes. The colour blue denotes a stable equilibrium solution, red denotes an unstable equilibrium solution with one negative eigenvalue of the tangential stiffness matrix, green denotes an unstable equilibrium solution with two negative eigenvalues of the tangential stiffness matrix. (For interpretation of the references to colour in this figure legend, the reader is referred to the Web version of this article.)

Rheinboldt allowed, for example, *loci* of bifurcation and/or limit points to be traced directly with respect to an additional parameter (load factor being the first) without having to compute an entire set of load-displacement curves.

During the mid 1990's, Eriksson and co-workers [24,32,33] established themselves as the main proponents and developers of generalised path-following, presenting numerous examples where the approach proved to be of great benefit, while also providing details on how the technique could be incorporated into commercial nonlinear finite element codes. More recently the technique has been embraced for the analysis of bistable plates and shells for morphing structures [34–36] and is also being considered as an optimisation tool [37].

In parallel, numerical bifurcation analysis techniques have been developed for generic dynamical systems, from the pioneering work of Doedel, Keller, and Kervenez [38,39], to cover a wide range of differential equations, including delay-differential equations [40], partial differential equations [41], integro-differential equations [42], and stochastic evolution equations [43]. We refer the readers to [44,45] for a recent review and tutorial, respectively.

The wealth of literature on each of the topics illustrates a considerable interest in the (in)stability of shallow arched structures; path-following of solutions in algebraic and differential equations; and also in structural optimisation, but there is little that brings together all three, this paper aims to do exactly that.

1.3. Aims and objectives

The aim of this paper is twofold. First, by means of an exploratory exercise we investigate the mechanics of compliant shallow arched structures to determine a shape-optimised arch for maximising the first instability load, and show that the design drivers for the nonlinear mechanics of arches are opposite to what would be expected from a linear analysis. Hence, the risks inherited in shells optimised with linear assumptions observed by Lee and Hinton are confirmed herein [46]. Second, we wish to illustrate how nonlinear structures with multi-parameter dependent characteristics can be designed robustly and quickly using a systematic approach. In this sense, the generalised path-following technique is introduced as an advanced design and analysis tool which can be used to explore a bounded multi-dimensional design space within a finite element context. The overarching aim is to further evolve the engineer's capability to design structures by employing nonlinearities to potentially extend the concept of structural efficiency into the nonlinear elastic regime or include additional functionality by exploiting compliance and large reversible deformations which may replace more complex mechanisms.

The remaining sections of the paper are structured as follows. Section 2 introduces a general overview of the mathematical framework of coupling the numerical continuation technique to the nonlinear finite element method. Section 3 discusses the application of the generalised path-following framework to a shallow arched beam problem, presents the results obtained and provides a discussion of key findings. The problem definition is presented, followed by a robust four-parameter analysis of the structural response. The cross-sectional area is distributed along the beam span, and this optimum distribution is then analysed further by evaluating the effect of arch mass and arch rise height on the structural response, whereby the optimality criterion is defined as the maximum stiffness before instability occurs.

2. Problem formulation

In principle, it is desirable to understand how structures behave when one or more design parameter are varied. During the design of engineering structures, parametric studies are the conventional approach, whereby multiple simulations for different configurations are performed. Generally speaking, analytical methods are more popular for these parametric studies, as they are less computationally demanding than finite element methods and therefore allow for quicker iteration in the evaluation of the design space. For nonlinear problems, analytical techniques that allow rapid parametric design are found wanting such that the design space investigated is often restricted. In a nonlinear setting, robust computational tools for parametric studies are therefore indispensable and the generalised path-following technique is presented here as such a tool to investigate the entire design space.

Consider a classic force-displacement equilibrium path of an arch loaded by a transverse point load at its mid-span, as illustrated in Fig. 1a. The mid-span applied load is parametrised and the corresponding vertical displacement of the centre is measured. The chosen colour code denotes the degree of instability of the system. The blue segments of the curve correspond to stable equilibrium paths (all eigenvalues of the tangential stiffness matrix are positive), red segments denote one unstable mode (one negative eigenvalue) and green segments denote two unstable modes (two or more negative eigenvalues). The points separating different colour segments are called critical points, *i.e.* points where at least one eigenvalue of the tangential stiffness matrix is exactly zero, and these can either be saddle-node bifurcation points (limit points), pitchfork bifurcation points, or a coincidence of both known as hilltop-branching points with two zero eigenvalues.

A saddle-node bifurcation (limit) point describes an extremal point (maximum or minimum) with respect to the control parameter, where equilibrium of the system switches from stable to unstable, or vice versa, but symmetry of the system is maintained. As the control parameter increases (or decreases) beyond a limit point, the structure snaps to an adjacent stable equilibrium state at the specified load, as shown by the dotted arrow. On the contrary, at a pitchfork bifurcation point the symmetry of the system is broken such that a secondary equilibrium path branches away from the fundamental path (not shown in Fig. 1a). Depending on the stability of this bifurcating branch, stable or unstable, the structure may transition onto this path or snap to another stable point. In Fig. 1a, the maximum limit point precedes the bifurcation point for a typical loading history starting from the unloaded state, but this is not necessarily always the case, and the order in which they appear may reverse for other configurations.

From this didactic example we can deduce particular points that are of interest to the engineer of practical nonlinear structures: (i) limit loads that induce snapping, (ii) bifurcation points that lead to branch switching or snapping, and (iii) classical design points where critical stress values or displacement values are exceeded. To optimise the nonlinear structure (for any given criteria – weight, cost, strength, *etc.*), it is important to understand the variables (material properties, geometric dimensions, *etc.*) that affect the structural response. More specifically, how do these variables affect the characteristics of the aforementioned three solution points?

Conventional design philosophy requires a complete re-analysis of the problem with different values for each variable. The re-evaluation of the structural behaviour can be avoided, however, when using generalised path-following. The comprehensive computational framework is discussed by Eriksson [33] (also see Ref. [47]), but in principle, an additional variable is introduced as a control parameter and the solution space explored in this third dimension using standard path-following techniques, see Fig. 1b, generating a two-dimensional surface. Therefore, the generalised path-following process involves tracing one-dimensional curves in a higher-dimensional solution space.

The conventional equilibrium of internal and external forces can be expressed as a function of a loading parameter, λ, and the displacement state variables, $\boldsymbol{u}$, in the form:

$$\boldsymbol{F}(\boldsymbol{u}, \lambda) = \boldsymbol{f}(\boldsymbol{u}) - \boldsymbol{p}(\lambda) = \boldsymbol{0}, \tag{1}$$

where $\boldsymbol{p}(\lambda)$ is the external (non-follower) load vector and $\boldsymbol{f}(\boldsymbol{u})$ is the internal force vector. For generalised path-following, Eq. (1) is adapted to incorporate any number of additional parameters, such that,

$$\boldsymbol{F}(\boldsymbol{u}, \boldsymbol{\Lambda}) = \boldsymbol{f}(\boldsymbol{u}, \boldsymbol{\Lambda}_1) - \boldsymbol{p}(\boldsymbol{\Lambda}_2) = \boldsymbol{0}, \tag{2}$$

where $\boldsymbol{\Lambda} = [\boldsymbol{\Lambda}_1^\top, \boldsymbol{\Lambda}_2^\top]^\top = [\lambda_1, \ldots, \lambda_p]^\top$ is a vector containing p control variables. $\boldsymbol{\Lambda}_1$ corresponds to parameters that influence the internal forces (*e.g.* material properties, geometric dimensions, temperature and moisture fields) and $\boldsymbol{\Lambda}_2$ relates to externally applied mechanical loads (*e.g.* forces, moments, tractions).

The n number of equilibrium equations in Eq. (2), correspond directly to the n number of displacement degrees of freedom in the system. Because the structural response is parametrised by p additional parameters a p-dimensional solution manifold in $\mathbb{R}^{(n+p)}$ exists, named *the equilibrium surface* by Sewell [25]. By defining additional auxiliary equations, $\boldsymbol{g}$, specific solution subsets on the p-dimensional solution manifold are defined. Hence, we wish to evaluate solutions to the augmented system

$$\boldsymbol{G}(\boldsymbol{u}, \boldsymbol{\Lambda}) \equiv \begin{pmatrix} \boldsymbol{F}(\boldsymbol{u}, \boldsymbol{\Lambda}) \\ \boldsymbol{g}(\boldsymbol{u}, \boldsymbol{\Lambda}) \end{pmatrix} = \boldsymbol{0}. \tag{3}$$

For r auxiliary equations, the solution to Eq. (3) becomes $(p - r)$-dimensional and hence $p - 1$ auxiliary equations are required to define a one-dimensional curve. As outlined by Eriksson [33] these subset equations can define fundamental equilibrium paths, *i.e.* the fundamental load parameter is varied and all other parameters are constant; secondary equilibrium paths (parameter paths), *i.e.* a different parameter is varied; bifurcation branching paths (pitchfork bifurcation paths); critical paths where the tangential stiffness matrix is singular (foldline path); *etc.*

Throughout this paper we exclusively evaluate one-dimensional curves, such that $r = p - 1$. This means that one additional constraining equation needs to be specified to uniquely solve the system of equations for a point on the curve. Hence, a specific solution $\boldsymbol{\nu} = (\boldsymbol{u}, \boldsymbol{\Lambda})$ on the subset curve is determined from

$$\boldsymbol{G}^N(\boldsymbol{\nu}) \equiv \begin{pmatrix} \boldsymbol{F}(\boldsymbol{\nu}) \\ \boldsymbol{g}(\boldsymbol{\nu}) \\ N(\boldsymbol{\nu}) \end{pmatrix} = \boldsymbol{0}, \tag{4}$$

where N is a scalar equation which plays the role of a multi-dimensional arc length constraint throughout the continuation along a specific subset curve. A specific solution to Eq. (4) is determined by a consistent linearisation coupled with a Newton-Raphson algorithm

$$\boldsymbol{\nu}_{j+1} = \boldsymbol{\nu}_j - \left(\boldsymbol{G}^N_{,\boldsymbol{\nu}}(\boldsymbol{\nu}_j)\right)^{-1} \cdot \boldsymbol{G}^N(\boldsymbol{\nu}_j), \tag{5a}$$

with

$$\boldsymbol{G}^N_{,\boldsymbol{\nu}} = \begin{pmatrix} \boldsymbol{F}_{,\boldsymbol{u}} & \boldsymbol{F}_{,\boldsymbol{\Lambda}} \\ \boldsymbol{g}_{,\boldsymbol{u}} & \boldsymbol{g}_{,\boldsymbol{\Lambda}} \\ N^\top_{,\boldsymbol{u}} & N^\top_{,\boldsymbol{\Lambda}} \end{pmatrix}, \tag{5b}$$

where j corresponds to the *jth* increment and the comma notation has been used to denote differentiation.

For visualisation purposes it is convenient to reduce the dimensionality of the presented results from $(n + p)$-dimensional solution space to a more palatable two- or three-dimensional space. The approach used for this is to consider a particular norm of the displacement field, *e.g.* the displacement at a specific point of interest $u = u_{\text{ref}}$, and to continue solution subsets in one parameter at a time.

As a result, all figures presented herein are shown in two or three dimensional plots. More precisely, we will visualise results by projecting them on a space $(\lambda_i, d(\boldsymbol{u})) \in \mathbb{R}^2$, or on a space $(\lambda_i, d(\boldsymbol{u}), \lambda_j) \in \mathbb{R}^3$, where λ_i and λ_j are suitably chosen control parameters, and where $d(\boldsymbol{u})$ is the displacement of the computed equilibrium at λ_i or (λ_i, λ_j). The choice of control parameters will be made explicit in all cases, whereas we will henceforth suppress the dependence of d on $\boldsymbol{u}$ for notational convenience.

From an algorithmic viewpoint, we have opted for a simple yet affordable choice: we compute one-parameter families of equilibria (in the parameter λ_i), as the secondary parameter λ_j is held constant, and we repeat the calculation for various values of λ_j. In this way, we parametrise the solution manifold using level sets at constant λ_j. An attractive alternative approach (which has not been pursued here for simplicity) is to cover the solution manifold with polygons, as proposed by Henderson [48] and implemented in the software package MULTIFARIO. In some instances, however, it is also possible to compute loci of branching points as λ_i and λ_j vary simultaneously, using standard two-parameter continuation of bifurcation points.

3. Instability analysis using generalised path-following

We now proceed to the evaluation of the arched beam structure, using generalised path-following techniques to elucidate physical insight into the underlying mechanics of the system. A shallow arched beam with *encastré* boundary conditions at either end, ubiquitous in the structural mechanics literature [49–51], is an ideal problem for this purpose.

The basic model is illustrated in Fig. 2a for a circular cross-section with baseline quantities of height-to-span ratio of 1/10, an axial rigidity of $EA = 6.5 \times 10^{11}$N, a shear rigidity $GA = 2.8275 \times 10^{11}$N, a bending rigidity $EI = 1.68107 \times 10^{11}$Nm. Additionally, some of the arch characteristics are explicitly defined as active parameters that can be varied throughout the analysis. These four parameters are the loading factor, λ_1, quadratic distribution of cross-sectional area, λ_2 (See Fig. 2b), average cross-sectional area (defined as a ratio of bending and axial rigidity $EI/EA = A/4\pi$), λ_3, and arch height normalised by span, λ_4 which are detailed in Table 1. The baseline geometry of the arch is defined as $\lambda_2 = 1$ (no spanwise variation of the cross-section), circular cross-sectional area with $\lambda_3 = I/A = 0.2586$ and arch height normalised by span $\lambda_4 = 0.1$.

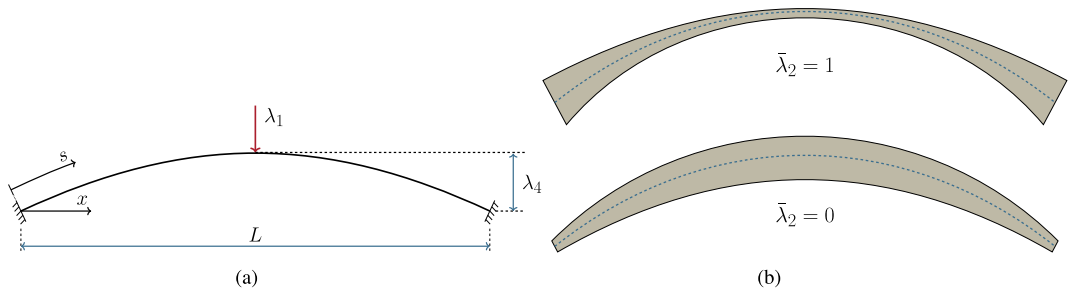

Fig. 2. Schematic diagram of the cylindrical arch with (a) describing geometry, boundary condition and applied loading, and (b) the control variable λ_2, which governs the distribution of cross-sectional area along the arch span.

Table 1
List of parameters used to investigate the nonlinear structural behaviour of the arch.

Parameter	Quantity	Units	$\lambda_i^{\min}$	$\lambda_i^{\max}$
λ_1	Loading factor	[−]	0	300
λ_2	Quadratic spanwise area distribution	[−]	0.999515	1.00095
λ_3	Average cross-sectional area	[m^2]	0.2586	0.5570
λ_4	Arch height-to-span ratio	[−]	0	0.1

For generality, the parameters are linearly mapped to a unit domain for post-processing, such that

$$J(\lambda,\overline{\lambda}) : [\lambda_i^{\min},\lambda_i^{\max}] \rightarrow [\overline{\lambda}_i^{\min},\overline{\lambda}_i^{\max}] = [0,1],$$
$$J(\lambda,\overline{\lambda}) = \overline{\lambda}_i^{\min} + \frac{\left(\lambda_i^{*}-\lambda_i^{\min}\right)\left(\overline{\lambda}_i^{\max}-\overline{\lambda}_i^{\min}\right)}{\lambda_i^{\max}-\lambda_i^{\min}} = \overline{\lambda}_i^{*}, \tag{6}$$

where λ_i^* is an arbitrary value of λ_i within the pre-defined bounds outlined in Table 1.

The problem is solved via a simple one-dimensional finite element formulation using fifty quadratic, three node, nonlinear Timoshenko beam elements with von Kármán strains (See Ref. [52] for formulation). This element choice is merely for simplicity as the model arch problem considered here is governed by moderate rotations. Indeed initial convergence studies showed that more elaborate beam formulations, *e.g.* the finite strain theory by Reissner [53], produced identical results for the constitutive and geometric parameters studied throughout. The mechanics of slender shallow arches are typically governed by snap-through instabilities and not material nonlinearities. The analysis is therefore restricted to only geometrical nonlinearities, however the strains are assessed throughout the loading history to ensure elastic behaviour is maintained. Finally, geometric symmetry of the structure is not exploited to reduced computational expense as this eliminates the possibility of asymmetric bifurcations.

3.1. Instabilities with varying arch height, λ_4

The preliminary process in using the generalised path-following technique requires the solution of a fundamental load-displacement equilibrium path for a baseline problem. As defined above the baseline configuration corresponds to $\lambda_2 = 1$, $\lambda_3 = 0.2586$ m^2 and $\lambda_4 = 0.1$ and for this configuration the solution path illustrates the classic snap-through behaviour illustrated in Fig. 1a.

It is from this fundamental path that other parameters are now explored. For every solution point on the fundamental path it is possible to follow a one-dimensional subset equilibrium curve, expanding the design space from a single-parameter space (λ_1-d), to a dual-parameter space (λ_1-d-λ_i).

Fig. 3 shows how the load-displacement response (λ_1 versus mid-span displacement d) varies with arch height. For $\overline{\lambda}_4 = 0$ the arch reduces to a flat beam, whereas for $\overline{\lambda}_4 = 1$ the arch height-to-span ratio is at a maximum 1/10. Curves (I) and (II) shown in the bottom plot of Fig. 3 represent the load-displacement response for these two extremal values of $\overline{\lambda}_4$, respectively. Hence, as the rise of the arch increases the structural behaviour smoothly transitions from curve (I) to curve (II), where the former is indicative of nonlinear bending of a flat beam and the latter of symmetric snap-through behaviour of an arched beam.

From Fig. 3 it is evident that arch height significantly affects the structural behaviour, and this is depicted by the chosen colour code. As previously defined, blue curves denote stable equilibria, red curves denote one unstable mode and green curves two unstable modes. As indicated by the blue region, the flat beam is stable throughout the entire loading range, $\lambda_1 \in [0, 150]$, and this remains the case for very shallow arches. A limit point is first observed for an arch height of $\overline{\lambda}_4 = 0.1155$, which relates to a height-to-span ratio of 0.0115. This point is clearly visible by the appearance of red curve segments in Fig. 3

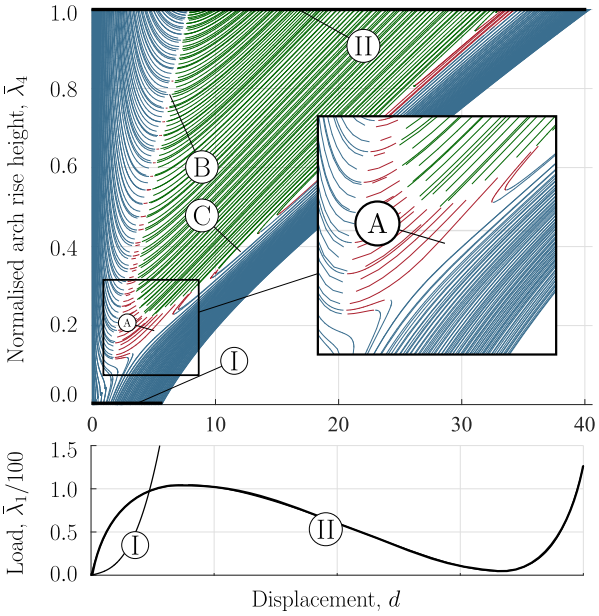

Fig. 3. Parameter $\overline{\lambda}_4$, corresponding to the normalised arch-height, is varied from a minimum of zero, *i.e.* a flat beam, to a maximum of 0.1, corresponding to a height-to-span ratio of 10%. I and II correspond to the load-displacement curves at a height-to-span ratio of zero and 1/10, respectively. The colours blue denote a stable equilibrium solution path, red denote an unstable equilibrium solution with one negative eigenvalue of the stiffness matrix, and green denotes an unstable equilibrium solution with two negative eigenvalues of the stiffness matrix. (For interpretation of the references to colour in this figure legend, the reader is referred to the Web version of this article.)

and is characterised by a broken pitchfork bifurcation in the $\lambda_4 - d$ plane. As the arch height increases further an additional instability arises denoted by green curve segments, which corresponds to a bifurcation point on the fundamental load-displacement path. The first limit point and first bifurcation points asymptotically converge (see point B in Fig. 3), however they do not cross for the parameter range investigated here. However, there is a coincident point of the limit and bifurcation loads present in Fig. 3 which illustrates this exact phenomenon of two instabilities converging and then diverging (point C).

In many engineering applications of arch structures, height is a design specification and therefore fixed *a priori*. From the results presented in Fig. 3 it may already be possible to design for the application in mind, however, in the event that the load carrying capacity or the deformations sustained are not appropriate for the given application, further evaluation is required. Parameters λ_2 and λ_3 are now introduced to tailor the structural response to a specific application.

3.2. Optimising distribution of mass, λ_2

The second parameter λ_2, evaluated herein relates to the distribution of cross-sectional area along the span of the arch.

A quadratic distribution of the cross-sectional area symmetric about the mid-span is implemented as follows,

$$A(\bar{s}) = a\bar{s}^2 + c, \tag{7}$$

where $\bar{s} = s/S$ is the arc-length co-ordinate normalised to total arch-length, S, with $\bar{s} = 0$ at the mid-span, and $\bar{s} = [-0.5, 0.5]$ at the two ends. Therefore the total arch volume, V, is given by

$$V = \int_{-0.5}^{0.5} \left(a\bar{s}^2 + c\right)\, d\bar{s} = \frac{a}{12} + c \quad \Rightarrow c = V - \frac{a}{12}, \tag{8}$$

which means that the distribution of the cross-sectional area reduces to

$$A(\bar{s}) = a\left(\bar{s}^2 - \frac{1}{12}\right) + V, \tag{9}$$

where the total volume, V, is conserved throughout the rest of the analysis, *i.e.* mass is conserved. The parameter that varies the distribution of area is defined by $\lambda_2 = 1 + a$ and certain limits need to be imposed on a to enforce that the cross-sectional area remains positive. Thus, for reducing area towards the ends $A(\bar{s} = \pm 0.5) > 0$, and similarly for reducing area towards the mid-span $A(\bar{s} = 0) > 0$. These constraints result in the following limits on a,

$$-6V < a < 12V. \tag{10}$$

A physical connection between the distribution of area and the distribution of second moment of area is maintained with $I(s) = \alpha A^2$, where $\alpha = 1/4\pi$, which means that a circular cross-section is assumed throughout all analyses. Although Eq. (10) represents the bounds of a, additional precautions were taken to constrain the limits further in order to maintain a well-conditioned numerical system. The two extreme physical configurations of $\bar{\lambda}_2$ are conceptually illustrated in Fig. 2b, to be used as reference when referring to the results presented in Fig. 4a.

Fig. 4a presents three distinct regions, each corresponding to a different degree of stability: blue, stable equilibria; red, one unstable mode; green, two or more unstable modes. Of course, the red and green segments of the equilibrium path are unstable and therefore of relatively little practical use to the practical engineer, but it is often important to include these regions as they are important for imperfection sensitivity. Increased awareness of the characteristics of the unstable regions mitigates the uncertainty, and thus improving the robustness, of prospective designs. Furthermore, awareness of the unstable regions becomes far more significant for dynamic behaviour and thus a complete investigation of these regions is important.

Nevertheless, we would like to point out that some configurations exhibit highly nonlinear solutions, as is the case for $\bar{\lambda}_2 = 0$, whose load-displacement curve is shown in Fig. 4b. This load-displacement response exhibits numerous "flower petals" and for each limit point (maximum or minimum) the arch transitions to a different mode shape, *i.e.* the number of half-waves across the span changes. Hence, the solid green line corresponds to degree of instability two with three half-waves along the span, and the broken green line corresponds to a third degree of instability or greater with five or more half-waves across the span. These observations agree with the findings presented by Pi *et al.* [54]. Additional bifurcation points are also observed on the dashed curve, but omitted here for clarity. Second, we note that Fig. 4b shows that the bifurcation points, when compared to the baseline configuration (Fig. 1a), have migrated along the equilibrium path and are now

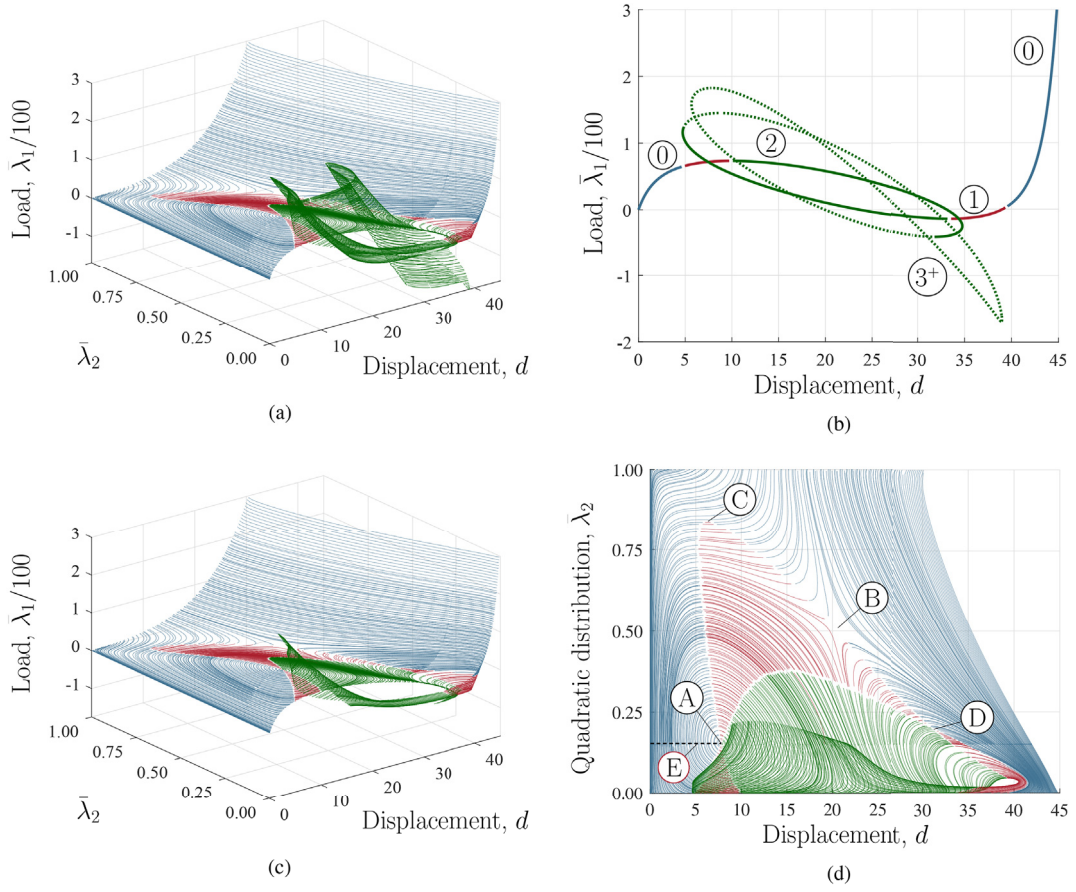

Fig. 4. (a) Solution surface in $\bar{\lambda}_1$-displacement-$\bar{\lambda}_2$ space of an arched beam with a height-to-span ratio of 1/10. Coefficient $\bar{\lambda}_2$ corresponds to the normalised symmetric quadratic distribution of cross sectional area along the length of the beam. For $\bar{\lambda}_2 = 0$ the arch is thinnest at the ends and for $\bar{\lambda}_2 = 1$ it is thinnest at the mid-span. Blue: Stable; Red: Unstable, one negative eigenvalue; Green: Unstable: two or more negative eigenvalues; (b) Load-displacement solution path for $\bar{\lambda}_2 = 0$ with degree of instability denoted in circles; (c) and (d) Partial solution surface for $0 < \bar{\lambda}_2 < 1$ highlighting points of interest (A) Peak, (B) Bifurcation in λ_2, (C) Snap-through initiates (cusp), (D) Limit point and bifurcation points coincide (hilltop-branching point). (For interpretation of the references to colour in this figure legend, the reader is referred to the Web version of this article.)

observed *before* the limit points – restricting the stable, useful design space.

Removing all solutions with degrees of instability three and above from the surface solution in Fig. 4a produces a somewhat clearer representation of the available design space as illustrated in Fig. 4c and d, where Fig. 4c is an isometric projection of the equilibrium surface, and Fig. 4d is an orthographic projection in the $\overline{\lambda}_2$-displacement plane. Fig. 4d shows a number of interesting points. Point (A) corresponds to the greatest peak before snap-though, and thus the greatest load-carrying capacity, therefore presenting the optimum load-carrying configuration (in terms of maximum λ_1/d ratio). Point (B) illustrates a bifurcation in $\overline{\lambda}_2$ space. Point (C) represents the value of $\overline{\lambda}_2$ for which snap-through behaviour first occurs. Point (D) indicates a single point where a bifurcation point has merged with a limit point to form a so-called hilltop branching point, *i.e.* where the fundamental path transitions from stable equilibrium to equilibrium with two unstable modes. Finally, dashed-line (E) corresponds to the configuration of $\overline{\lambda}_2 = 0.154525$ with the greatest stiffness through deformation *i.e.* maximum λ_1/d which reaches its maximum at the first instability load at point (A).

Given that engineering structures are typically designed for maximum load carrying capacity and minimum deflection for a given mass, the distribution of cross-sectional area corresponding to $\overline{\lambda}_2 = 0.154525$ is defined as the most efficient design. This particular configuration is characterised by a redistribution of mass from the supported edges to the centre of the arch, *i.e.* distribution of mass towards the centre of the beam and away from the boundary conditions. This is not necessarily an intuitive finding, and merits further discussion.

For comparison, the results for three different distributions were evaluated, (i) constant cross-section $\overline{\lambda}_2^{\text{const}} = 0.337979$, (ii) optimum distribution $\overline{\lambda}_2^{\text{opt}} = 0.154525$, and (iii) inverse-optimum distribution $\overline{\lambda}_2^{\text{inv}} = 0.521433$. The inverse-optimum configuration was defined as the inverse of the optimum value for λ_2 when compared to the constant area $\lambda_2 = 1$ ($a = 0$), such that,

$$\lambda_2^{\text{inv}} = \lambda_2^{\text{const}} + \left(\lambda_2^{\text{const}} - \lambda_2^{\text{opt}}\right), \tag{11}$$

transformed to the normalised $\overline{\lambda}_2^{\text{inv}}$ parameter value using Eq. (6).

The critical buckling loads for all three configurations were found to vary significantly, $\lambda_{1,\text{crit}}^{\text{const}} = 91.97$, $\lambda_{1,\text{crit}}^{\text{opt}} = 104.5$ and $\lambda_{1,\text{crit}}^{\text{inv}} = 67.15$. At the respective critical buckling loads the overall deformation of the arch was evaluated (See Fig. 5a) alongside the internal membrane energy Π_{m} (Fig. 5b) and membrane forces N_x (Fig. 5c and d), as well as the bending energy (Fig. 5e) and bending moments (Fig. 5f and g).

As a result of reaching 1.56 times the critical snap-through load, the optimum configuration deforms more than the inverse-optimum configuration at the point of snap-through (see Fig. 5a). As this relative increase in deformation is considerably less than the 1.56 times increase in load, the stiffness of the optimum configuration is greater than the inverse-optimum configuration. The mode shape of the optimum configuration also suggests that the deformation is more uniform over the central portion of the arch where snap-through occurs, suggesting that the internal loads are being re-distributed to use the available material more efficiently.

In fact, the distribution of the membrane forces over the arch span can provide further physical insight into the optimal distribution of the cross-sectional area. It is well known that many structural instabilities are driven by destabilising compressive membrane forces. The equilibrium equation of shallow arches using Donnell-Kármán kinematics is

$$\frac{d^2M_s}{ds^2} - \frac{N_s}{R} + N_s\frac{d^2w_0}{ds^2} = 0, \tag{12}$$

and given that $M_s = -EI(s)\frac{d^2w_0}{ds^2}$

$$\frac{d^2}{ds^2}\left(EI(s)\frac{d^2w_0}{ds^2}\right) + \frac{N_s}{R} - N_s\frac{d^2w_0}{ds^2} = 0, \tag{13}$$

where w_0 is the transverse displacement of the arch and N_s is the membrane force. Note that for a shallow arch N_x and N_s are basically indistinguishable. In the arch problem considered here, the transversely applied load at the mid-span forces the ends of the arch to expand outwards, but because this is prevented by the *encastré* boundary conditions a compressive reaction force is induced throughout the structure. As this compressive membrane force $-N_s$ increases (becomes more negative), the effective bending rigidity provided by EI is reduced until the arch loses its capability to support any form of transverse loading.

As the snap-through instability occurs at the mid-span of the arch, it intuitively follows that increasing the load carrying capability of the arch requires a re-distribution of the compressive membrane forces away from the mid-span and towards the supported edges. In fact, this mechanism is widely attributed to the improved load-carrying capability of variable-angle tow composite plates under compression [55]. Variable angle-tow plates are composite laminates manufactured from orthotropic plies with the reinforcing fibres steered continuously over the planform in curvilinear paths. As a result of this stiffness variation compressive stresses can be tailored, *i.e.* re-distributed from the central unsupported region of the plate to the supported edges, thereby significantly increasing the critical buckling load [55].

Precisely the same mechanism can be observed for the arch studied here. For example, consider the membrane energy in Fig. 5b. The constant cross-section (blue) provides a relatively constant membrane energy across the span. The optimum configuration (red) reduces the membrane energy over the critical mid-span region where snap-through occurs. It is clearly visible that membrane energy is distributed outwards away from the critical region and towards the supported edges. Furthermore, the opposite distribution membrane energy is observed for the inverse-optimum distribution – the membrane energy is maximised towards the centre.

The significance of this re-distribution is further emphasised in Fig. 5c and d, which respectively show the membrane force N_x along the length of the beam normalised by the respective critical buckling load and the reaction force N_x at the boundary. Fig. 5c shows that changes in distribution of cross-sectional area from the inverse-optimum configuration (thicker towards the boundaries) to a constant cross-sectional area and further to the optimum configuration (thicker towards the mid-span) reduces the magnitude of the compressive load across the arch. Furthermore, Fig. 5d illustrates that for the optimum design not only the magnitude of the compressive load is reduced at the critical mid-span region, but the distribution of N_x is also more uniform across the entire arch domain. Conversely, Fig. 5e–g shows that the optimum cross-sectional area distribution leads to a concentration of bending energy at the mid-span and greater magnitude of bending moment over most portions of the arch, thereby maximising the out-of-plane bending deformation before snap-through occurs as previously noted for Fig. 5a. Hence, the optimum area distribution redistributes some of the internal loading from membrane action to bending action.

The optimum design is found to be in agreement with the findings observed by Rapp [50], whereby the critical buckling loads are evaluated for non-uniform beams with three different volume distributions. The only case directly comparable to the results presented within this paper ($m = 2$ and $n = 2$ in Ref. [50]) agree with the findings herein.

The linear design of arch structures, such as masonry arches in antiquity, is often based on minimising bending moments and maximising the compressive thrust within the arch. This is because the mortar used to bind together the rigid links of the arch fare poorly under tensile loading. In this regard, a linear design of a masonry arch would be based on maximising the compressive membrane force throughout the structure. As shown in Fig. 5c the compressive membrane force is uniformly at the greatest value throughout the inverse-optimum structure. Hence, the inverse-optimum distribution (thicker at the boundaries and thinner towards the mid-span) could be viewed as an optimised design for masonry arches, and this is indeed the case for many arch bridges and aqueducts. This comparison illustrates the risks entailed in optimising

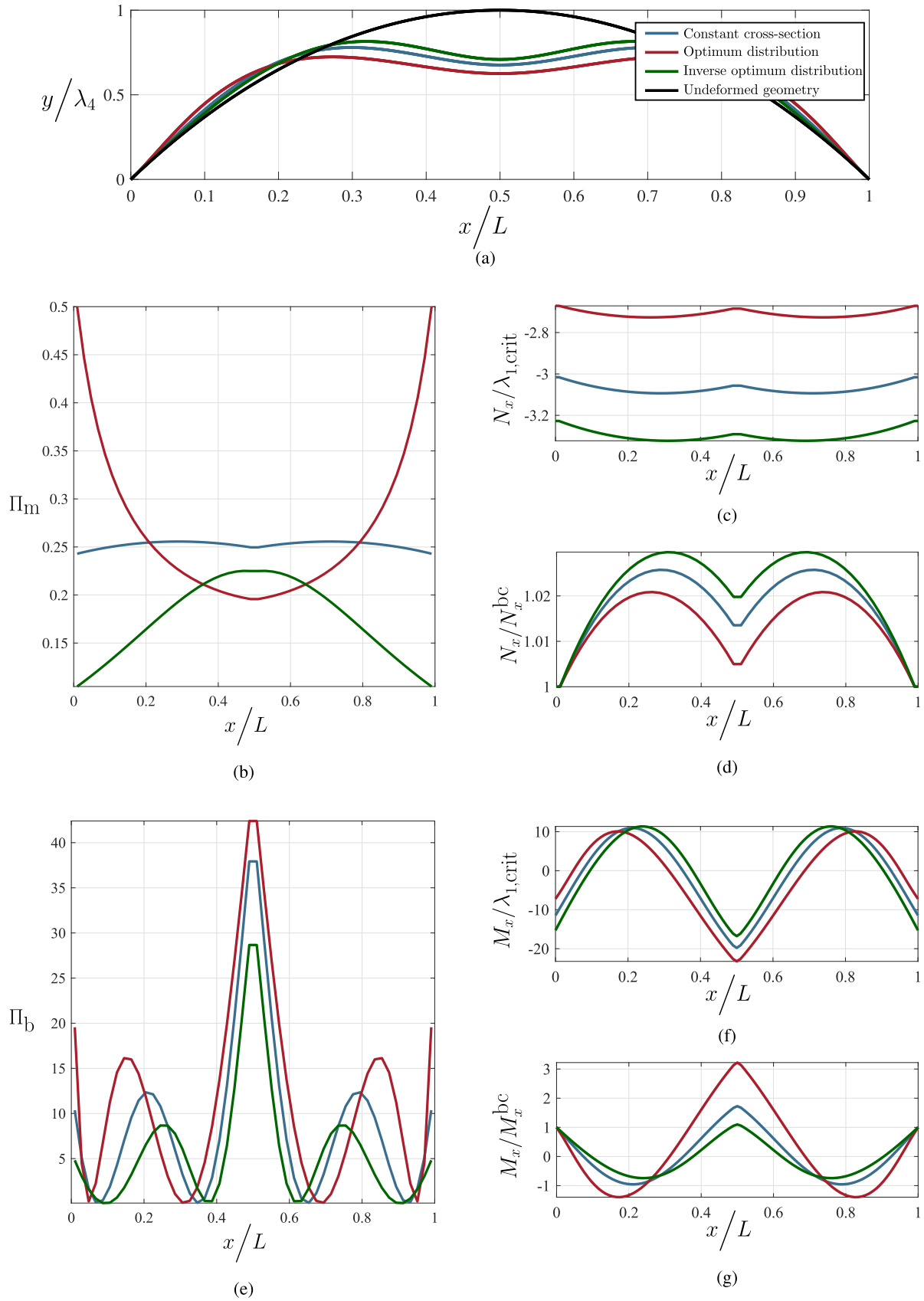

Fig. 5. Plots of the (a) Deformation of the arch, (b) Membrane energy, Π_m, (c) Membrane force, N_x, normalised with respect to critical buckling load, (d) Membrane force, N_x, normalised with respect to the reaction load at the boundary, (e) Bending energy, Π_b, (f) Bending moment, M_x, normalised with respect to critical buckling load, (g) Bending moment, M_x, normalised with respect to the reaction moment at the boundary, all at the critical buckling load. The red curves correspond to the optimum spanwise distribution of area, the blue corresponds to the constant spanwise area, and the green corresponds to the inverse-optimum spanwise distribution of area. (For interpretation of the references to colour in this figure legend, the reader is referred to the Web version of this article.)

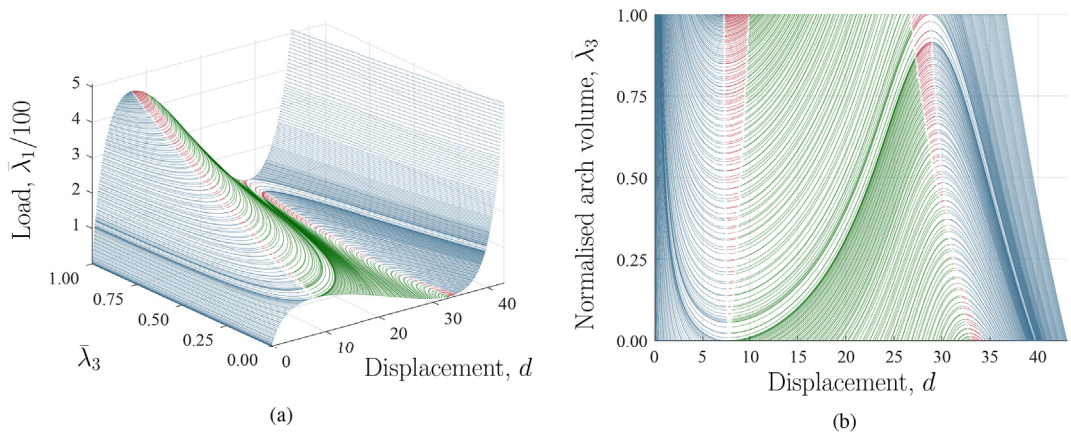

Fig. 6. Plots of the (a) Load-displacement behaviour of an arched beam with a height-to-span ratio of 1/10. Parameter λ_3 corresponds to the average cross-sectional area, and therefore relates directly to total volume of the beam. The average area is varied within bounds of $\lambda_3 = [0.2586, 0.5570]$, (b) An orthographic view of (a) in the $\overline{\lambda}_3$-displacement plane. Blue: Stable; Red: Unstable, one negative eigenvalue; Green: Unstable: two or more negative eigenvalues. (For interpretation of the references to colour in this figure legend, the reader is referred to the Web version of this article.)

elastic arches used in the nonlinear domain using linear assumptions, as the design driver, *i.e.* minimising the compressive thrust, is indeed opposite to that for most linear arches.

3.3. Changing total arch volume, λ_3

With an optimum mass distribution of $\overline{\lambda}_2 = 0.154525$ defined, the average cross-sectional area, parameter $\overline{\lambda}_3$, is now varied. As the width and density of the arch remain fixed, varying $\overline{\lambda}_3$ investigates the effect of increasing mass.

As the baseline model has been optimised, in terms of the distribution of volume, the original load-displacement equilibrium solution can no longer be used as a reference for further evaluation. It is therefore necessary to find the solution to the fundamental equilibrium path with parameter $\overline{\lambda}_2 = 0.154525$. This newly-created load-displacement path is then used as a starting point to expand the equilibrium surface into the λ_3-direction as shown in Fig. 6.

The maximum mass is defined for $\overline{\lambda}_3 = 1$ and the minimum mass corresponding to the previously optimised solution corresponds to $\overline{\lambda}_3 = 0$. Two important conclusions can be drawn from Fig. 6. First, the qualitative behaviour of the structure changes when volume is increased, *i.e.* snap-through becomes more nonlinear and thus physically more sudden. Second, the snap-through displacement increases inversely with volume, *i.e.* the snap-distance is greater for lighter arches.

Fig. 6 is a good example of a visual aid that is useful to the design engineer. The most important aspect of any structure is usually the load carrying capacity. Each equilibrium curve drawn in Fig. 6 represents a fixed load, and it is therefore possible to follow a given load to find a specified displacement before or even after snap-through has occurred. This technique allows engineers to design more efficient structures by fully exploiting nonlinear kinematics.

4. Conclusion

The aim of this investigation was to explore the mechanics of shallow arched beams using a computational framework known as generalised path-following, our objective being to illustrate the juxtaposition between the design of a *linear* and a *nonlinear* arch structure.

This investigation produces equilibrium surfaces of the structural behaviour which facilitate an intuitive understanding of the structural stability response with respect to any number of parameters, here the external load, distribution of mass, total mass and arch height. The design of this simple arch proves to be very sensitive to the investigated parameters. Nonlinear buckling behaviour of arched beams strongly depends on the arch rise height, the beam slenderness ratio, beam volume, and most interestingly the spanwise distribution of cross-sectional area. A quadratic distribution of a marginally thicker cross-section at the mid-span provides the greatest rigidity to a centrally applied bending load, *i.e.* the greatest load carrying capacity to displacement ratio. Although the analysis was restricted to only geometrical nonlinearities, the strain was assessed throughout the loading history and showed no sign of plasticity onset. Indeed, the mechanics of slender shallow arches are typically governed by snap-through instabilities and material nonlinearities are more important for higher arches.

Furthermore, we illustrate that the mechanics of shallow nonlinear circular arches are topologically opposed to that of the linear equivalent. It shows that there are essentially two approaches to designing arches. In many linear structures, such as masonry arches, the optimum design drives a re-distribution of mass to the supported boundary conditions, and thus a linear analysis tool is sufficient. For the nonlinear structure investigated here, the opposite is true as a redistribution of mass towards the mid-span reduces the destabilising compressive membrane force within the structure, which in turn increases the load-carrying capacity before the first instability is observed. This physical mechanism is analogous to variable angle tow plates, where compressive stresses are redistributed from the unsupported centre of the plate to supported edges. Finally, by redistributing mass the load-carrying capacity of the arch at the first instability load is increased by 14% over the baseline design of constant cross-sectional area.

Acknowledgement

The authors would like to acknowledge the Engineering and Physical Sciences Research Council (EPSRC) through the EPSRC Centre for Doctoral Training in Advanced Composites for Innovation and Science [grant number EP/G036772/1] and also the EPSRC Fellowship titled *Structural Efficiency and Multi-Functionality of Well-Behaved Nonlinear Composite Structures* [grant number EP/M013170/1].

Data Statement

All data required to reproduce the figures in this paper can be found on the data repository of the University of Bristol via URL: https://data.bris.ac.uk/data/.

References

[1] P.M. Reis, A perspective on the revival of structural (in)stability with novel opportunities for function: from buckliphobia to buckliphilia, J. Appl. Mech. 82 (11) (2015) 111001–1–11001–4.
[2] A. Carpinteri, F. Bazzucchi, A. Manuello, Nonlinear instability analysis of long-span roofing structures: the case-study of porta susa railway-station 110 48–58.
[3] R. C. Batra, M. Porfiri, D. Spinello, Review of modeling electrostatically actuated microelectromechanical systems 16.
[4] K. Das, R. C. Batra, Pull-in and snap-through instabilities in transient deformations of microelectromechanical systems 19.
[5] K. Das, R. C. Batra, Symmetry breaking, snap-through and pull-in instabilities under dynamic loading of microelectromechanical shallow arches 18.
[6] K.-E. Kurrer, The History of the Theory of Structures - from Arch Analysis to Computational Mechanics, first ed., Ernst & Sohn.
[7] S.A. Alkharabsheh, M.I. Younis, Statics and dynamics of mems arches under axial forces, J. Vib. Acoust. 135 (021007) (2013) 1–7.
[8] A. Rafsanjani, A. Akbarzadeh, D. Pasini, Snapping mechanical metamaterials under tension, Adv. Mater. 27 (39) (2015) 5931–5935.
[9] O. C. Zienkiewicz, Short communications and comment: incremental displacement in nonlinear analysis 3 587–592.
[10] J.-L. Batoz, G. Dhatt, Incremental displacement algorithms for nonlinear problems 14(8) 1262–1267.
[11] Y. T. Feng, D. Peric, D. R. J. Owen, A new criterion for determination of initial loading parameter in arc-length methods 58 (3) 479–485.
[12] Y. T. Feng, D. Peric, D. R. J. Owen, Determination of travel directions in path-following methods 21 (7) 43–59.
[13] K.-J. Bathe, E. N. Dvorkin, On the automatic solution of nonlinear finite element equations 17 (5–6) 871–879.
[14] G. Powell, J. Simons, Improved iteration strategy for nonlinear structures 17 1455–1467.
[15] G. A. Wempner, Discrete approximations related to nonlinear theories of solids 7 1581–1599.
[16] E. Riks, The application of Newton's method to the problem of elastic stability 39(4) 1060–1065.
[17] M. A. Crisfield, A fast incremental/iterative solution procedure that handles "snap-through" 13 55–62.
[18] J. T. Gierlinski, T. R. Graves Smith, A variable load iteration procedure for thin-walled structures 21(5) 1085–1094.
[19] S.E. Leon, A unified library of nonlinear solution schemes, Appl. Mech. Rev. 64 (2011) 1–26.
[20] H. B. Keller, Lectures on Numerical Method in Bifurcation Problems, Tata Institute of Fundamental Research, Lectures Delivered at the Indian Institute of Science, Bangalore.
[21] E. J. Dodel, A. R. Champneys, T. F. Fairgrieve, Y. A. Kuznetsov, B. Sandstede, X. Wang, AUTO 97: Continuation and Bifurcation Software for Ordinary Differential Equations (With HomCont).
[22] Y. Kuznetsov, Elements of Applied Bifurcation Theory, 3rd Edition, Vol. 112 of Applied Mathematical Sciences, Springer, 2004.
[23] R. Seydel, Practical Bifurcation and Stability Analysis, 3rd Edition, Vol. 5 of Interdisciplinary Applied Mathematics, Springer-Verlag New York, 2010.
[24] A. Eriksson, Structural instability analyses based on generalised path-following, Comput. Methods Appl. Mech. Eng. 156 (1998) 45–74.
[25] M. J. Sewell, On the connection between stability and the shape of the equilibrium surface 14 203–230.
[26] M. J. Sewell, Some mechanical examples of catastrophe theory 12 163–172.
[27] J. M. T. Thompson, Bifurcation Aspects of Catastrophe Theory 553–571 Part VI: Engineering.
[28] J. M. T. Thompson, Catastrophe theory in mechanics: progress or digression 10 (2) 167–175.
[29] W. C. Rheinboldt, Numerical analysis of continuation methods for nonlinear structural problems 13 103–113.
[30] W. C. Rheinboldt, Numerical Analysis of Parameterized Nonlinear Equations, first ed., Volume 1 of The University of Arkansas Lecture Notes in the Mathematical Sciences, Wiley-Blackwell.
[31] W. C. Rheinboldt, On the computation of multi-dimensional solution manifolds of parametrized equations 53 165–181.
[32] A. Eriksson, Fold lines for sensitivity analyses in structural instability, Comput. Methods Appl. Mech. Eng. 114 (1994) 77–101.
[33] A. Eriksson, Equilibrium subsets for multi-parametric structural analysis, Comput. Methods Appl. Mech. Eng. 140 (1997) 305–327, http://www.sciencedirect.com/science/article/pii/S0045782596010961.
[34] A. Pirrera, D. Avitabile, P.M. Weaver, Bistable plates for morphing structures: a refined analytical approach with high-order polynomials, Int. J. Solid Struct. 47 (2010) 3412–3425.
[35] A. Pirrera, D. Avitabile, P.M. Weaver, On the thermally induced bistability of composite cylindrical shells for morphing structures, Int. J. Solid Struct. 49 (2012) 685–700, http://www.sciencedirect.com/science/article/pii/S0020768311003933.
[36] R. Groh, A. Pirrera, Generalised path-following for well-behaved nonlinear structures, Comput. Methods Appl. Mech. Eng. 331 (2018) 394–426.
[37] A. Eriksson, Constraint paths in non-linear structural optimization, Comput. Struct. 140 (2014) 39–47, http://www.sciencedirect.com/science/article/pii/S0045794914001096.
[38] E. Doedel, H.B. Keller, J.P. Kernevez, Numerical analysis and control of bifurcation problems (i): bifurcation in finite dimensions, Int. J. Bifurc. Chaos 1 (03) (1991) 493–520.
[39] E. Doedel, H.B. Keller, J.P. Kernevez, Numerical analysis and control of bifurcation problems (ii): bifurcation in infinite dimensions, Int. J. Bifurc. Chaos 1 (04) (1991) 745–772.
[40] K. Engelborghs, T. Luzyanina, D. Roose, Numerical bifurcation analysis of delay differential equations using dde-biftool, ACM Trans. Math. Softw. (TOMS) 28 (1) (2002) 1–21.
[41] L.S. Tuckerman, D. Barkley, Bifurcation Analysis for Timesteppers, in: Numerical Methods for Bifurcation Problems and Large-scale Dynamical Systems, Springer, 2000, pp. 453–466.
[42] J. Rankin, D. Avitabile, J. Baladron, G. Faye, D.J. Lloyd, Continuation of localized coherent structures in nonlocal neural field equations, SIAM J. Sci. Comput. 36 (1) (2014) B70–B93.
[43] D. Avitabile, K. C. A. Wedgwood, Macroscopic coherent structures in a stochastic neural network: from interface dynamics to coarse-grained bifurcation analysis, J. Math. Biol.
[44] H. Osinga, J.G.-V.B. Krauskopf, Numerical Continuation Methods for Dynamical Systems, 2007.
[45] D. Avitabile, Numerical Computation of Coherent Structures in Spatially-extended Systems, 2015.
[46] S. Lee, E. Hinton, Dangers inherited in shells optimized with linear assumptions 78 473–486.
[47] A. G. Salinger, N. M. Bou-Rabee, R. P. Pawlowski, E. D. Wilkes, E. A. Burroughs, R. B. Lehoucq, L. A. Romero, LOCA 1.0 Library of Continuation Algorithms: Theory and Implementation Manual, Sandia National Laboratories.
[48] M.E. Henderson, Multiple parameter continuation: computing implicitly defined k-manifolds, Int. J. Bifurc. Chaos 12 (03) (2002) 451–476.
[49] Y. C. Fung, A. Kaplan, Buckling of Low Arches or Curved Beams of Small Curvature, National Advisory Committee for Aeronautics Technical Note 2840, National Advisory Committee for Aeronautics.
[50] I. H. Rapp, Snap-through Buckling of Shallow Arches with Nonuniform Stiffness under Dynamic and Quasi-static Loadings, Phd.
[51] Y.-L. Pi, N. S. Trahair, Non-linear buckling and postbuckling of elastic arches 20 (7) 571–579.
[52] J. N. Reddy, An Introduction to Nonlinear Finite Element Analysis, Oxford University Press.
[53] E. Reissner, On one-dimensional, large-displacement, finite strain beam theory, Stud. Appl. Math. 52 (1973) 87–95.
[54] Y.-L. Pi, M. A. Bradford, Y.-L. Guo, Revisiting nonlinear in-plane elastic buckling and postbuckling analysis of shallow circular arches under a central concentrated load 142 (8).
[55] Z. Gurdal, B. Tatting, C. Wu, Variable stiffness composite panels: effects of stiffness variation on the in-plane and buckling response 39 911–922.